Available online at www.sciencedirect.com
ScienceDirect
Journal of Power Sources 165 (2007) 427–435
JOURNAL OF POWER SOURCES
www.elsevier.com/locate/jpowsour

Short communication

Semi-empirical modeling of charge and discharge profiles for a $LiCoO_2$ electrode

Qi Zhang, Qingzhi Guo [1], Ralph E. White [*,2]

Department of Chemical Engineering, University of South Carolina, Columbia, SC 29208, USA

Received 9 November 2006; accepted 6 December 2006
Available online 20 December 2006

Abstract

The experimental charge and discharge profiles of a $LiCoO_2$ electrode show that the overpotential of the electrode does not change much during galvanostatic charge, but changes significantly during galvanostatic discharge. Semi-empirical porous electrode models are presented to simulate the charge and discharge profiles of the $LiCoO_2$ electrode. The symmetry factor is empirically assumed to decrease with the state of discharge of the electrode to enable the model predictions to agree well with the experimental discharge profiles.

Keywords: Lithium cobalt oxide electrode ($LiCoO_2$); Numerical simulation; Symmetry factor

1. Introduction

Lithium cobalt oxide has been widely used as cathode material in lithium ion secondary batteries. The reaction of $LiCoO_2$ is well known to be lithium ion extraction from and insertion into a layered cobalt dioxide matrix. Many researchers [1–3] have simulated the charge and discharge behaviors of a full cell sandwich which uses $LiCoO_2$ as cathode material. However, very few studies can be found in the literature focusing on $LiCoO_2$ electrode alone. In this work, the rate capability of a $LiCoO_2$ electrode was studied in half cells with a three-electrode setup. The study shows that the overpotential of the $LiCoO_2$ electrode does not change much during galvanostatic charge, but changes significantly with cell state of discharge during galvanostatic discharge. A pseudo-2D porous electrode model [4–6] was used to simulate charge and discharge profiles of the $LiCoO_2$ electrode. Empirical expressions were used in the Butler–Volmer equation to enable the model predictions to agree well with the experimental data.

2. Experiment

The rate capability of a $LiCoO_2$ electrode was measured using a Swagelok-type half cell (see Fig. 1). The half cell consisted of a $LiCoO_2$ working electrode, a separator and a lithium foil counter electrode. Cone shaped lithium metal with a sharp end was placed just above the $LiCoO_2$ electrode to serve as the reference electrode. The potential of the $LiCoO_2$ electrode *versus* Li/Li^+ was measured directly in the experiment. The working electrode was a round disc with a diameter of 1/2 in. pouched out of a singled-sided $LiCoO_2$ sheet electrode provided by Mine Safety Appliances (Sparks, MD). The Celgard-2300 polypropylene membrane (Charlotte, NC) of a thickness of 25 μm was used as the separator. The electrolyte (Ferro, Independence, OH) was 1.0 M $LiPF_6$ in a solvent mixture of EC/PC/EMC/DEC. The half cell was assembled in an argon-filled glovebox, removed and placed in a Tenney environmental chamber controlled at 15 °C. An 8-channel Arbin battery test unit was used to conduct the rate capability test.

The half cell was first cycled several times at the *C*/13 rate ($C = 4$ mA) between 3.0 and 4.35 V *versus* Li/Li^+ to stabilize the electrochemical performance of the $LiCoO_2$ electrode. The capacity of the $LiCoO_2$ disc electrode was measured around 4 mAha when it was cycled between the given voltage window. The currents used in rate capability test included 6×10^{-5}, 3×10^{-4}, 6×10^{-4}, 1.5×10^{-3} and 3×10^{-3} A, which roughly

* Corresponding author.
E-mail address: white@engr.sc.edu (R.E. White).
[1] Electrochemical Society Student Member.
[2] Electrochemical Society Fellow.

0378-7753/$ – see front matter © 2006 Elsevier B.V. All rights reserved.
doi:10.1016/j.jpowsour.2006.12.025

Nomenclature

a_s	specific interfacial area of the electrode ($cm^2\ cm^{-3}$)
Brug	Bruggeman coefficient
c_e	Li^+ concentration in the electrolyte ($mol\ cm^{-3}$)
c_s	solid phase Li^+ concentration in the $LiCoO_2$ electrode ($mol\ cm^{-3}$)
$c_{s,max}$	maximum solid phase Li^+ concentration in the $LiCoO_2$ electrode ($mol\ cm^{-3}$)
D_e	diffusion coefficient of the electrolyte ($cm^2\ s^{-1}$)
D_s	solid phase diffusion coefficient ($cm^2\ s^{-1}$)
$f_\pm$	mean molar salt activity coefficient
F	Faraday's constant, 96487 C mol^{-1}
i_0	exchange current density ($A\ cm^{-2}$)
I	applied current (A)
j	intercalation current density ($A\ cm^{-2}$)
k_p	kinetic rate constant ($A\ cm^{-2}\ (mol\ cm^{-3})^{-1.5}$)
Q	charge or discharge capacity (Ah)
R	gas constant, 8.3145 J $(mol\ K)^{-1}$
R_f	contact resistance ($\Omega\ cm^2$)
R_s	particle radius of the $LiCoO_2$ electrode (cm)
S	geometric area of the electrode (cm^2)
t	time (s)
t_+^0	transference number of the electrolyte
T	temperature (K)
U_{eq}	equilibrium potential of the electrode (V)
v	thermodynamic factor of the electrolyte
W	active material loading in the electrode (g)
x	x in Li_xCoO_2, SOC of the electrode

Greek letters

α_a, α_c	transfer coefficients
β	symmetry factor
δ_p, δ_s	electrode or separator thickness (cm)
ε_e, ε_s	volume fraction of the electrolyte or active material in solid phase
κ_e	conductivity of the electrolyte ($S\ cm^{-1}$)
σ_s	conductivity of the solid phase ($S\ cm^{-1}$)
ϕ_e, ϕ_s	liquid or solid phase potential (V)

Subscripts or superscripts

c, d	charge or discharge
eff	effective value
n, p	positive or negative electrode
sep	separator

correspond to the *C*/66, *C*/13, *C*/7, *C*/2.7, and *C*/1.3 rates, respectively. For rate capability test at *C*/66 rate, a single stage constant current protocol was used to charge and discharge the half cell. For other rates, a two stage constant current protocol was used. The cell was first charged or discharged to the desired voltage limit (3.0 or 4.35 V) using the target rate. Then a small current (*C*/66 rate) was applied to continue charge or discharge until the desired voltage limit was reached again. The use of the two

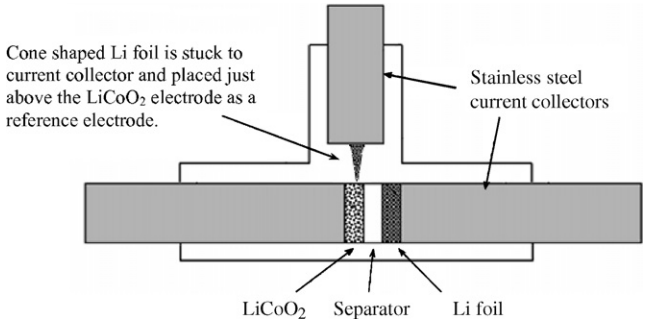

Fig. 1. Schematic of $LiCoO_2$ half cell setup used in the experiment. The reference electrode is used to measure the potential of the $LiCoO_2$ electrode.

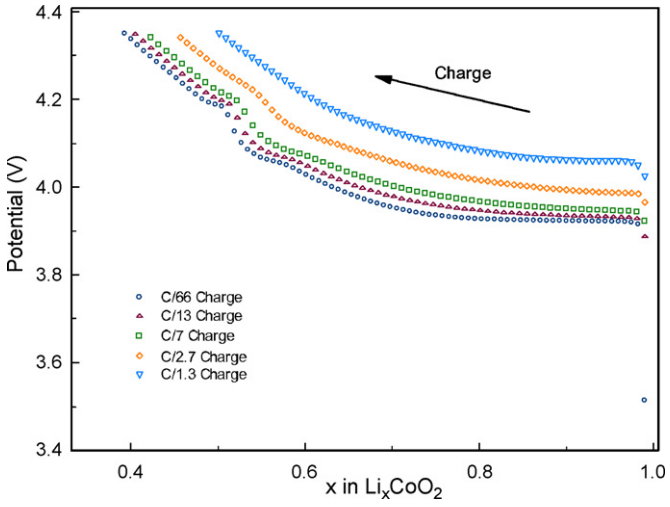

Fig. 2. Experimental galvanostatic charge profiles of the $LiCoO_2$ half cell ($C = 4$ mA).

stage charge/discharge protocol was to ensure the cell to reach the same SOC at the beginning of charge or discharge for all tests.

The charge and discharge profiles of the $LiCoO_2$ electrode are presented in Figs. 2 and 3 where the potential is plotted against x

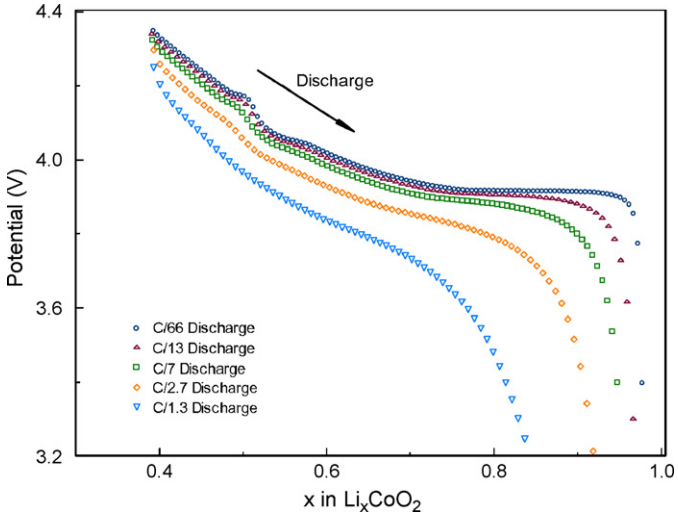

Fig. 3. Experimental galvanostatic discharge profiles of the $LiCoO_2$ half cell ($C = 4$ mA).

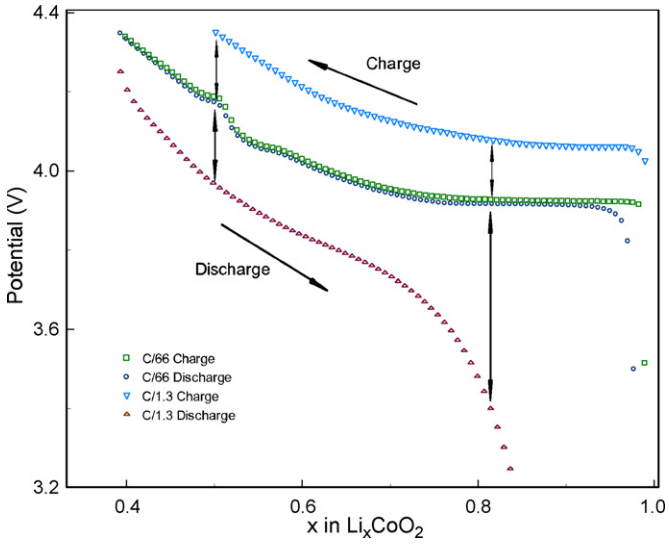

Fig. 4. The electrochemical behavior of the $LiCoO_2$ electrode is different during charge from that during discharge. The overpotential increases with x during galvanostatic discharge, but does not vary much during galvanostatic charge ($C = 4$ mA).

in Li_xCoO_2. The value of x in Li_xCoO_2 was calculated by using the following formula:

$$x = x_0 \pm \frac{Q}{0.274 \times W} \tag{1}$$

where W was the active material loading of the $LiCoO_2$ disc electrode and was determined to be 0.0245 g from disc electrode size and loading data provided by manufacture. The factor of 0.274 was the theoretical capacity in Ah to convert 1 g $LiCoO_2$ completely to CoO_2. The accumulative charge or discharge capacity Q in Ah was obtained directly from experimental data. The initial state (x in Li_xCoO_2) of the $LiCoO_2$ electrode was determined to be 0.99 for charge and 0.393 for discharge from low rate potential profiles.

The potential profiles of the $LiCoO_2$ electrode measured during the first stage charge process are compared with those measured during the first stage discharge process in Fig. 4 for both the C/66 and C/1.3 rates. As seen in Fig. 4, the potential profile measured during charge at the C/66 rate almost overlays with the potential profile measured during discharge at the same rate, which indicates that the electrode is very close to equilibrium. Unfortunately, this is not true for the C/1.3 rate. Several observations can be made by comparing the C/66 and C/1.3 rate charge and discharge profiles: First, the overpotential (relative to the equilibrium potential determined by averaging the C/66 rate potentials measured in both charge and discharge) does not change much during galvanostatic charge for both the C/66 and C/1.3 rates. But it exhibits heavy dependence on state of discharge (SOD) during discharge. Second, the potential of the $LiCoO_2$ electrode starts to drop at high SOD when the discharge rate is low. But it happens at low SOC if discharge rate is high. Third, the potential plateau around $x = 0.5$ (in Li_xCoO_2) gradually disappears in both charge and discharge profiles when the current is increased. Many researchers [7–9] explained the potential plateau in that region by a phase transition or equilibrium between ordered and disordered lithium ions in the CoO_2 framework. The movement of large amounts of lithium ions in a short time at high current rates may prevent this phase equilibrium from occurring, which would explain the gradual disappearance of the potential plateau at $x = 0.5$. And lastly, the $LiCoO_2$ electrode does not exhibit good rate capability, because it reaches the cutoff voltage early at low cell SOD when current rate is relatively high (C/1.3).

3. Model

Porous electrode models [4–6] have been heavily used in the literature to study the performance of lithium ion battery systems. A detailed explanation about porous electrode model used here can be found elsewhere [5,6]. The model equations are summarized below for the convenience of the readers.

The mass transport in solid $LiCoO_2$ particles is described by using Fick's diffusion law:

$$\frac{\partial c_s}{\partial t} = \frac{1}{r^2}\frac{\partial}{\partial r}\left(D_s r^2 \frac{\partial c_s}{\partial r}\right) \tag{2a}$$

$$-D_s \frac{\partial c_s}{\partial r}\bigg|_{r=0} = 0 \tag{2b}$$

$$-D_s \frac{\partial c_s}{\partial r}\bigg|_{r=R_s} = \frac{j}{F} \tag{2c}$$

A mass balance on the lithium ions in the solution phase yields:

$$\frac{\partial \varepsilon_e c_e}{\partial t} - \nabla \cdot (D_e^{\text{eff}} \nabla c_e) - \frac{1 - t_+^0}{F} a_s j = 0 \tag{3}$$

where the specific interfacial area of the electrode is $a_s = 3\varepsilon_s / R_s$.

The potential distributions in solid and solution phases are described as follows:

$$\nabla \cdot (\sigma_s \nabla \phi_s) - a_s j = 0 \tag{4}$$

$$\nabla \cdot \left(\kappa_e^{\text{eff}} \nabla \phi_e - \frac{2RT\kappa_e^{\text{eff}}}{F}(1 - t_+^0)\left(1 + \frac{\mathrm{d}\ln f_\pm}{\mathrm{d}\ln c_e}\right)\nabla \ln c_e\right) + a_s j = 0 \tag{5}$$

The concentrations and potentials in the solid and solution phase are coupled together through the intercalation current density j which is calculated through the Butler–Volmer equation:

$$j = i_{0,p}\left(\exp\left(\frac{\alpha_a F}{RT}(\phi_s - \phi_e - U_{eq} - jR_f)\right) - \exp\left(-\frac{\alpha_c F}{RT}(\phi_s - \phi_e - U_{eq} - jR_f)\right)\right) \tag{6a}$$

where the exchange current density $i_{0,p}$ is formulated as:

$$i_{0,p} = k_p c_e^{\alpha_a}(c_{s,\max} - c_s|_{r=R_s})^{\alpha_a} c_s|_{r=R_s}^{\alpha_c} \tag{6b}$$

The computation schematic of a half cell sandwich is shown in Fig. 5. The boundary conditions are thus given as:

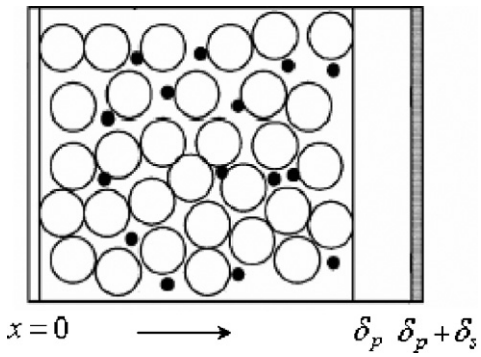

Fig. 5. Schematic of a $LiCoO_2$ half cell sandwich, consisting of $LiCoO_2$ cathode, separator and lithium foil anode.

- At $x = 0$:

$$-D_{e,pos}^{eff}\frac{\partial c_e}{\partial x} = 0 \tag{7a}$$

$$-\sigma_{s,pos}\frac{\partial \phi_s}{\partial x} = \frac{I}{S_p} \tag{7b}$$

$$-\kappa_{e,pos}^{eff}\frac{\partial \phi_e}{\partial x} = 0 \tag{7c}$$

- At $x = \delta_p$:

$$-D_{e,pos}^{eff}\frac{\partial c_e}{\partial x}\bigg|_{x=\delta_p^-} = -D_{e,sep}^{eff}\frac{\partial c_e}{\partial x}\bigg|_{x=\delta_p^+} \tag{8a}$$

$$-\sigma_{s,pos}^{eff}\frac{\partial \phi_s}{\partial x}\bigg|_{x=\delta_p^-} = 0 \tag{8b}$$

$$-\kappa_{e,pos}^{eff}\frac{\partial \phi_e}{\partial x}\bigg|_{x=\delta_p^-} = -\kappa_{e,sep}^{eff}\frac{\partial \phi_e}{\partial x}\bigg|_{x=\delta_p^+} \tag{8c}$$

- At $x = \delta_p + \delta_s$:

$$\frac{I/S_{sep}}{F}(1 - t_+^0) = -D_{e,sep}^{eff}\nabla c_e \tag{9a}$$

$$\frac{I}{S_{sep}} = -i_{0,n}\left[\exp\left(\frac{0.5F}{RT}(0 - \phi_e)\right) - \exp\left(\frac{-0.5F}{RT}(0 - \phi_e)\right)\right] \tag{9b}$$

The model equations (Eqs. (2)–(9)) were discretized in space using finite difference and solved using the DASSL subroutine in Fortran.

The properties of the $LiPF_6$ based electrolyte, such as diffusion coefficient and conductivity are important model parameters. But no experimental data were found in the literature for the electrolyte system used in this study (1.0 M $LiPF_6$ in the EC/PC/EMC/DEC mixture). Valoen and Reimers [10] measured the properties of $LiPF_6$ as a function of temperature and concentration in a slightly different electrolyte system which is $LiPF_6$ in a PC/EC/DMC mixture. Their results were used here in the simulation assuming that $LiPF_6$ behaves similarly in those two electrolytes. The diffusion coefficient of the electrolyte was found to be [10]:

$$\log(D_e) = -4.43 - \frac{54}{T - 5 \times 10^3 c_e - 229} - 0.22 \times 10^3 c_e \tag{10a}$$

The expression for the conductivity of the electrolyte was found to be [10]:

$$\kappa_e = c_e\begin{pmatrix}-10.5+0.074T - 6.96 \times 10^{-5}T^2 + 668c_e \\ -17.8c_eT+0.028c_eT^2 + 4.94 \times 10^5 c_e^2 - 886c_e^2T\end{pmatrix}^2 \tag{10b}$$

The effective value of the diffusion coefficient and conductivity of the electrolyte were used in the simulation to account for the actual path length of the species in porous media. They were calculated through Bruggeman's correlation:

$$D_e^{eff} = D_e\varepsilon_e^{Brug} \tag{11a}$$

$$\kappa_e^{eff} = \kappa_e\varepsilon_e^{Brug} \tag{11b}$$

The thermodynamic factor which account for the non-ideality of the electrolyte was found to be [10]:

$$v = (1 - t_+^0)\left(1 + \frac{\mathrm{d}\ln f_\pm}{\mathrm{d}\ln c_e}\right) = 0.601 - 7.59c_e^{0.5} + 3.1 \times 10^4(2.53 - 0.0052T)c_e^{1.5} \tag{12}$$

4. Simulation

4.1. Simulation on charge profiles of the $LiCoO_2$ electrode

Fig. 6 presents a comparison of the experimental data with the predicted charge curve using model equations presented above. Clearly, the model predictions do not agree with the

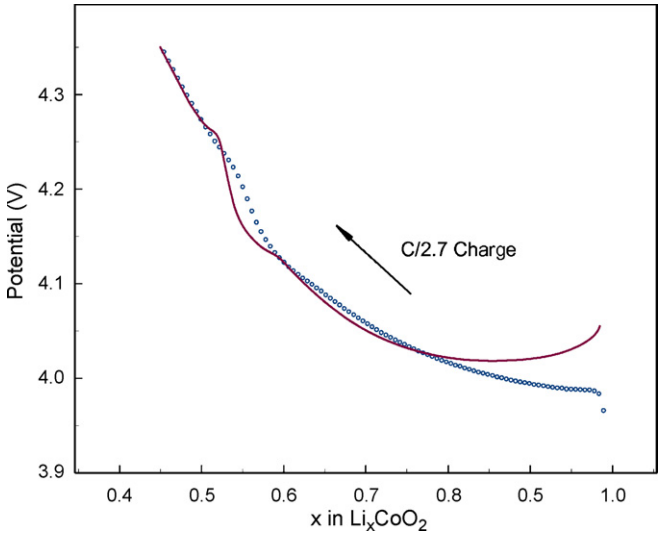

Fig. 6. The pseudo-2D model predicts an incorrect potential profile at the beginning of charge, especially from $x = 1.0$ to $x = 0.8$. Symbols represent experimental results. Line represents the simulation result.

Table 1
. Model parameters used to obtain Fig. 6

Parameter	Value	Parameter	Value
$LiCoO_2$ electrode			
T (°C)	15[a]	R_s (cm)	10×10^{-4}[b]
W (g)	0.0245[a]	Brug	1.5[b]
δ_p (cm)	64×10^{-4}[a]	D_s ($cm^2\ s^{-1}$)	2.8×10^{-10}[c]
S_p (cm^2)	1.267[a]	R_f ($\Omega\ cm^2$)	200[c]
ε_e	0.30[a]	$x_{0,p}$	0.99[c]
ε_s	0.60[a]	R_f ($\Omega\ cm^2$)	200[c]
σ_s ($S\ cm^{-1}$)	0.1[b]	$k_{p,c}$ ($A\ cm^{-2}\ (mol\ cm^3)^{-1.5}$)	4.2×10^{-2}[c]
t_+^0	0.363[b]		
Separator			
$c_{e,0}$	1×10^{-3}[a]	S_{sep} (cm^2)	1.267[a]
δ_s (cm)	25×10^{-4}[a]	ε_e	0.46[b]
D_e	Eq. (10a)	κ_e	Eq. (10b)
$(1-t_+^0)\left(1+\frac{d\ln f_\pm}{d\ln c_e}\right)$	Eq. (12)		

[a] Manufacture data or experiment data.
[b] From Refs. [1–3].
[c] Values fit to experiment data.

experimental data for $x \geq 0.8$. The model parameters used in the simulation are listed in Table 1. The exchange current density $i_{0,p}$ expression and the flat open circuit potential (OCP) of $LiCoO_2$ from $x \approx 0.75$–1 was found to be the combined cause of lack of agreement. Fig. 7 shows that the change of $i_{0,p}$ with x during the simulation where it can be seen that $i_{0,p}$ has a small value at the beginning of charge because $c_{s,max} - c_s|_{r=R_s}$ is close to zero, which causes the Butler–Volmer equation to predict a large overpotential for the set current density. As $i_{0,p}$ gradually increases during charge because $c_{s,max} - c_s|_{r=R_s}$ is becoming larger, the Butler–Volmer equation predicts a smaller overpotential for the same current density. The exchange current density in Eq. (6b) was derived based on the assumption of a close relation with the Nernstian form of the OCP [4]. However, the OCP of $LiCoO_2$ around $x \approx 0.75$–1 is highly non-Nernstian because it shows weak dependence on the lithium ion concentration in the solid matrix (see low rate profiles in Fig. 4). To address this problem, the concentration of empty sites $c_{s,max} - c_s|_{r=R_s}$ at the surface of solid particle is removed from exchange current density expression and the $i_{0,p}$ expression becomes:

$$i_{0,p} = k_p c_e^{\alpha_a} c_s|_{r=R_s}^{\alpha_c} \tag{13}$$

Eq. (13) means that the charge kinetics has a relatively strong dependence on the concentration of Li^+ occupied sites in $LiCoO_2$ but week (or no) dependence on the concentration of empty site, similar to kinetics in desorption process.

Fig. 8 compares the experimental and simulated charge profiles of the $LiCoO_2$ electrode using Eq. (13) for $i_{0,p}$ instead of Eq. (6b). Model parameters used in the simulation are listed in Table 2. Simulation results show good agreement with experiment ones for all charge rates. This study shows that with only constant model parameters, the model could predict sat-

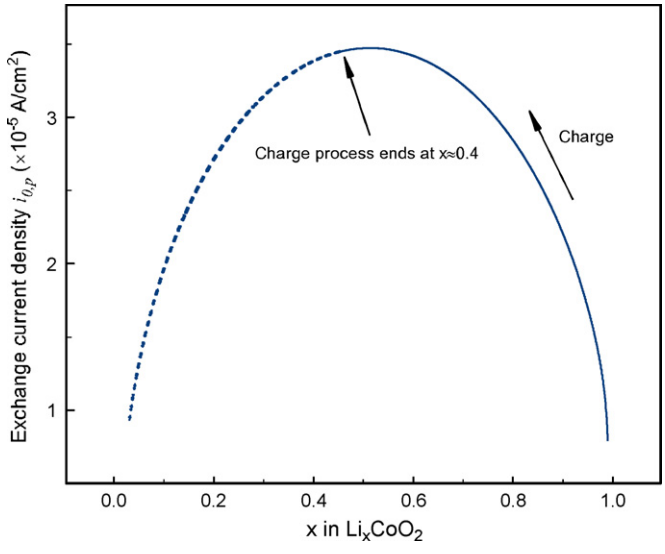

Fig. 7. Change of exchange current density $i_{0,p}$ with cell SOC when simulating Fig. 6.

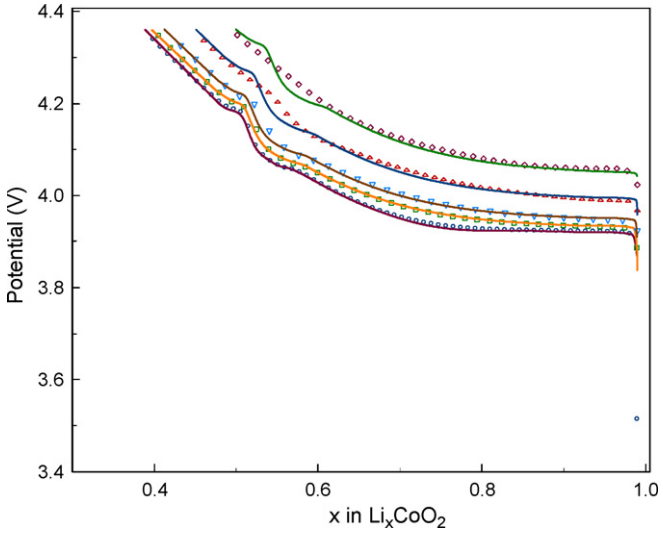

Fig. 8. Comparison of experiment (symbols) and simulated (lines) charge profiles at different current rates. The rates from bottom to top: *C*/66, *C*/13, *C*/7, *C*/2.7, and *C*/1.3 (*C* = 4 mA).

Table 2
Model parameters used to obtain Fig. 8[a] using Eq. (13)

Parameter	Value	Parameter	Value
$k_{p,c}$ ($A\,cm^{-2}\,(mol\,cm^3)^{-1}$)	6.0×10^{-3}[b]	$x_{0,p}$	0.99[b]

[a] Refer to Table 1 for parameters not listed here.
[b] Values fit to experiment data.

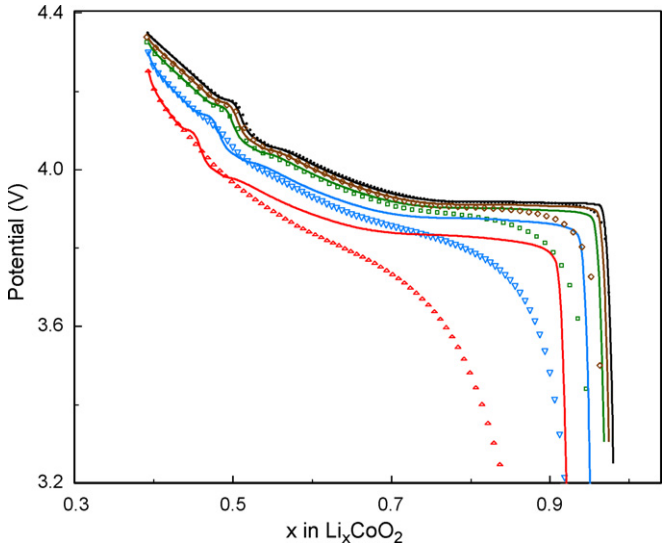

Fig. 9. The best simulation results (lines) obtained when model parameters are constants. The rates from top to bottom are *C*/66, *C*/13, *C*/7, *C*/2.7 and *C*/1.3 ($C = 4$ mA).

isfactorily the charge profiles of the $LiCoO_2$ electrode where overpotential does not vary much with SOC. The model could not predict the disappearance of the voltage plateau around $x = 0.5$ at high current rates because it does not include any mechanism to account for the phenomena.

4.2. Simulation on discharge profiles of the $LiCoO_2$ electrode

Fig. 9 shows the simulation results when the model parameters are kept constant during discharge using Eq. (6b) for $i_{0,p}$. The parameters used in the simulation are listed in Table 3. The simulated results fit the experiment profiles well at the beginning of discharge and when current rates are low. But the model failed to predict the increased potential drop with cell SOD at high rates. Extensive simulations indicate that it is very difficult for the model to predict experimental discharge profiles when all model parameters are kept constant except those for the electrolyte (Eqs. (10) and (12)).

Table 3
Model parameters used to obtain Fig. 9[a] using Eq. (6b)

Parameter	Value	Parameter	Value
D_s ($cm^2\,s^{-1}$)	1.4×10^{-10}[b]	$x_{0,p}$	0.393[b]
$k_{p,d}$ ($A\,cm^{-2}\,(mol\,cm^{-3})^{-1.5}$)	0.25[b]		

[a] Refer to Table 1 for parameters not listed here.
[b] Values fit to experiment data.

In order to achieve a better fit on discharge profiles, an empirical expression was introduced to the kinetic expression and used along with porous electrode model. The symmetry factor of the Li^+ insertion reaction is assumed to decrease with SOD based on our observation of increased potential drop during galvanostatic discharge. The Li^+ insertion reaction is usually considered as one electron transfer process.

$$Li^+ + \dot{S} + e^- \rightleftharpoons Li - S \tag{14}$$

The symmetry factor represents the fractional charge that promotes the cathodic reaction [4]. When symmetry factor β decreases with SOD, it physically implies that the reversible lithium ion intercalation reaction favors more the anodic reaction (Li oxidation) than it does the cathodic reaction (Li^+ reduction). That is, it becomes kinetically less favorable to insert Li^+ into the electrode as discharge goes on, which requires increased driving force, kinetic overpotential, to maintain the galvanostatic discharge current forced by the external circuit. The empirical expression for the symmetry factor β used is as follows:

$$\beta = 0.5\left(1 - \frac{1}{1+\exp(a(b - c_s|_{r=R_s}/c_{s,max}))}\right) \tag{15a}$$

$$\alpha_c = \beta \tag{15b}$$

$$\alpha_a = 1 - \beta \tag{15c}$$

Fig. 10 shows the simulation predicted potential profiles during the discharge of the $LiCoO_2$ electrode at different rates. The solid lines represent the simulated profiles and the symbols represent experimental data. Model parameters used to obtain Fig. 10 are listed in Table 4. Simulation results show good agreement with experimental data for all conditions. There is a significantly improvement over the previous case (Fig. 9) when the symmetry factor is allowed to decrease with SOD. The model well captures the fine details of experiment profiles at the beginning of discharge. The discharge profile of the $LiCoO_2$ electrode

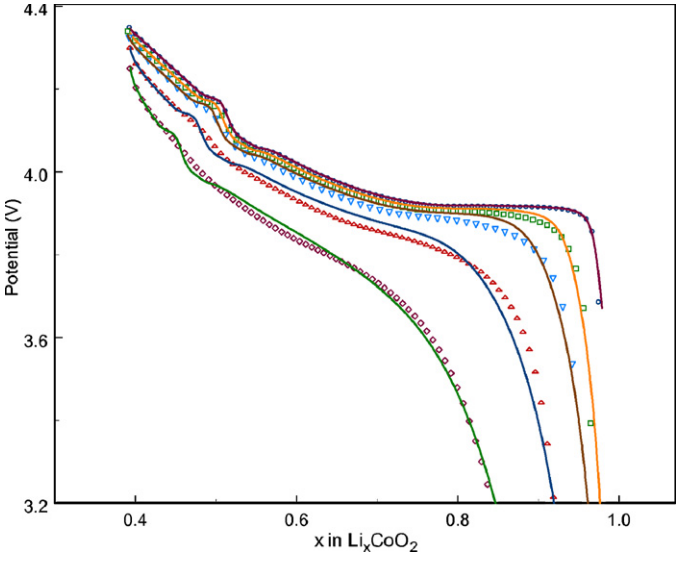

Fig. 10. Comparison of experiment (symbols) and simulation (lines) discharge profiles at different current rates. Symmetry factor β is assumed to decrease with cell SOD in galvanostatic discharge.

Table 4
Model parameters used to obtain Fig. 10[a]

Parameter	Value	Parameter	Value
D_s ($cm^2\ s^{-1}$)	1.2×10^{-10}[c]	$x_{0,p}$	0.393[c]
$k_{p,d}$ ($A\ cm^{-2}\ (mol\ cm^{-3})^{-1.5}$)	0.25[c]		

	Parameters used in Eq. (15)	
	a[d]	b[d]
$C/66$[†]	35	0.95
$C/13$	28	0.94
$C/7$	21	0.92
$C/2.7$	13	0.88
$C/1.3$	8	0.8

[c,d] Values fit to experiment data.
[†] $C = 4$ mA.
[a] Refer to Table 1 for parameters not listed here.

is a straight line before x reaches 0.5 at $C/66$ rate. That straight line gradually turns into a curve with increased curvature at high rate, which could be an indication of increased solid phase diffusion limitation in the $LiCoO_2$ electrode. The model well predicts the shape change of the experimental profiles at the beginning of discharge using a relatively small solid phase diffusion coefficient. It does not predict the disappearance of voltage plateau around $x = 0.5$ at high rates for the same reason discussed earlier.

In order to use the discharge model in other simulations, the parameters a and b in symmetry factor expression need to be correlated to current rates. The values of a and b obtained from fitting experimental discharge profiles are plotted against current rate in Figs. 11 and 12, respectively. Parameter a is found to depend rationally on current rate and parameter b linearly. The correlation expressions can be found in Table 5. The model now could be used to predict discharge profiles of the $LiCoO_2$ electrode given a discharge current rate. It should be noted that the treatment offered in the work, the dependence of symmetry factor on the surface concentration, is empirical. Nonetheless, the semi-empirical model should yield sufficient good results

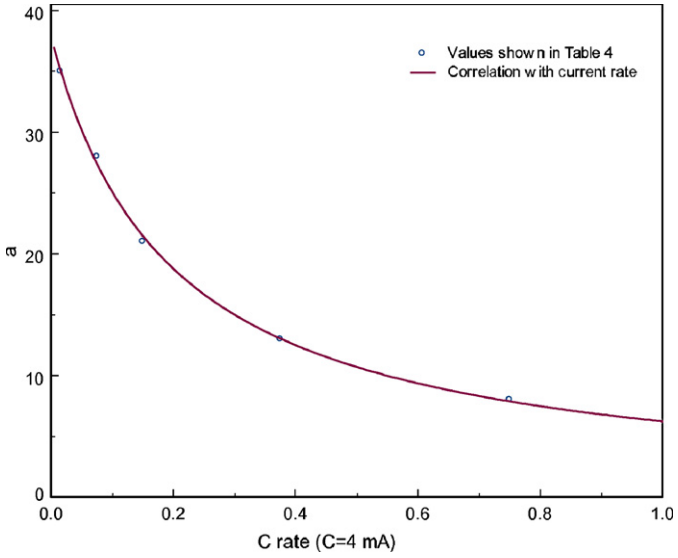

Fig. 11. The correlation of parameter a with current rate.

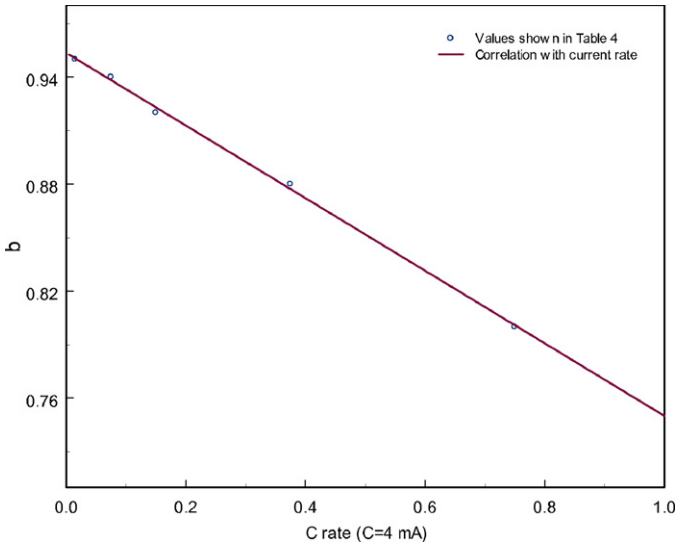

Fig. 12. The correlation of parameter b with current rate.

for electrode analysis provided that the operation conditions of the electrode are not varied to the extent that the empirical representation becomes substantially inaccurate.

4.3. Simulations using the models for $LiCoO_2$ electrode

In previous sections, porous electrode models were used to simulate experimental charge and discharge profiles of a $LiCoO_2$ electrode, which is the main purpose of the work. It is shown

Table 5
Correlations of parameters a and b for symmetry factor with current rate (x_c)

Parameter	Values with 95% confidence intervals
$a = a_1/(x_c + a_2)$	
a_1	7.453 ± 0.841
a_2	0.1969 ± 0.0285
$b = b_1 x_c + b_2$	
b_1	−0.2035 ± 0.014
b_2	0.9536 ± 0.0054

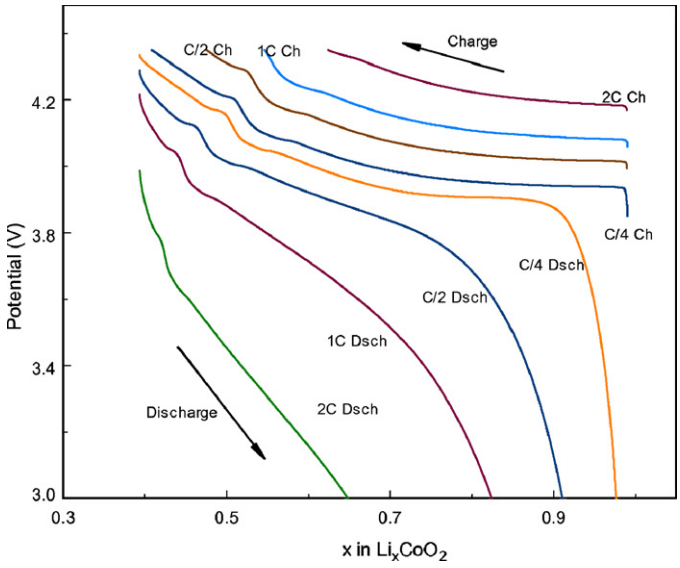

Fig. 13. Model predicted charge and discharge profiles for the $LiCoO_2$ electrode ($C = 4$ mA).

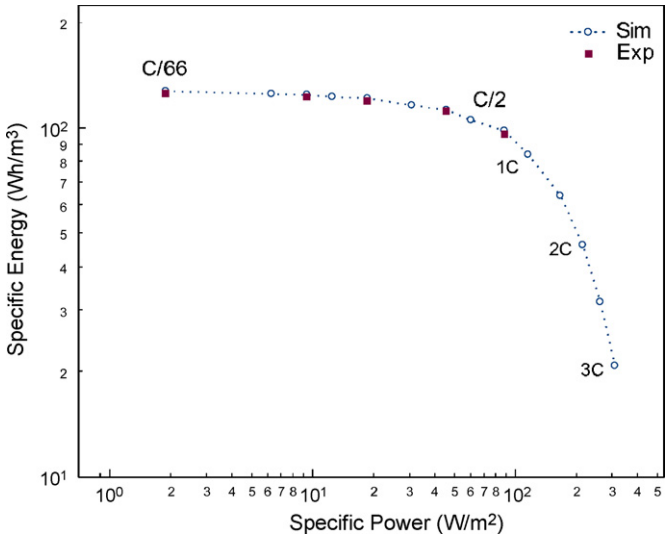

Fig. 15. Ragone plot of the $LiCoO_2$ electrode.

that simulation results agree well with experimental ones. With the availability of accurate models, one can study the electrochemical behaviors of the $LiCoO_2$ electrode in details.

The charge and discharge profiles of the $LiCoO_2$ electrode are simulated under different current rates and the results are shown in Fig. 13. The voltage window for the simulation is 3.0–4.35 V. The rate capacities are compared to the experiment values in Fig. 14. Simulation shows that the $LiCoO_2$ electrode used in the study does not exhibit a good rate capability in discharge. The model predicts the electrode can only achieve about 75% of the total capacity at 1 C rate and 50% at 2 C rate.

The rate capacity data can be converted into energy-power data to construct a Ragone plot which is a useful tool in comparing different battery designs. It is very time-consuming to construct such a plot experimentally. However, computer simulations can easily and rapidly generate a significant number of data points for a Ragone plot. The Ragone plot for the $LiCoO_2$ electrode is given in Fig. 15. The specific energy (Wh m^{-2}) and power (W m^{-2}) are higher than normal values because the electrode is charged to a higher SOC ($x \approx 0.4$) which could be the most direct way to increase specific energy and power. But in real-world applications, the $LiCoO_2$ electrode is rarely charged to such a high SOC because of the negative effect of phase transition at $x \approx 0.5$ on the life span of the electrode. The high end of charge voltage is used in the rate capability test to help us identify the solid phase diffusion limitation in the $LiCoO_2$ electrode from the shape change of discharge profiles. Ragone plot also shows that the electrode is not suited for applications where high rate discharge is needed because the specific energy of the electrode deteriorates quickly after the current passes 2 C.

The calculated salt concentration and solution phase potential profiles at 2 C rate are shown in Figs. 16 and 17, respectively. The profiles of the salt concentration show moderate concentration polarization. And diffusion coefficient of elec-

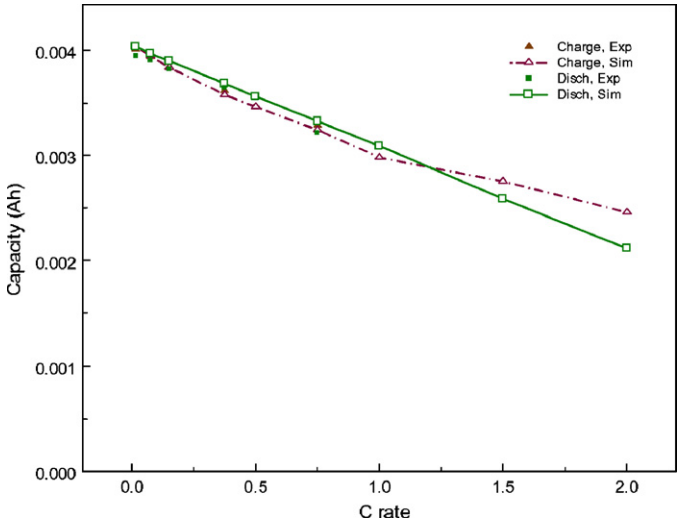

Fig. 14. Comparison of experiment and model predicted charge/discharge capacity.

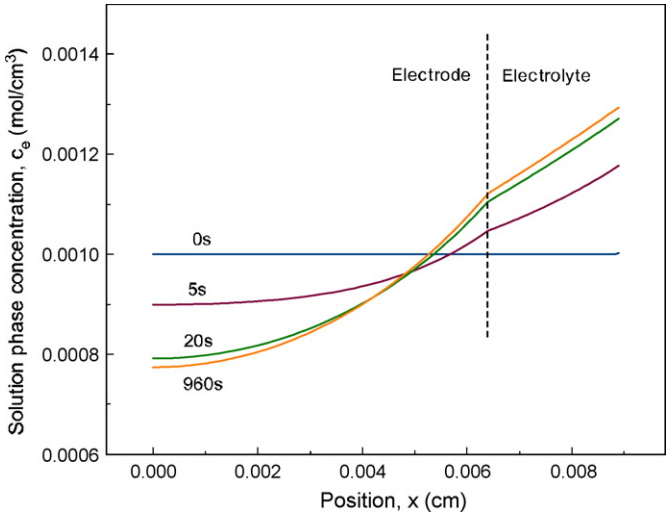

Fig. 16. Calculated solution phase concentration distribution at 2 C discharge rate.

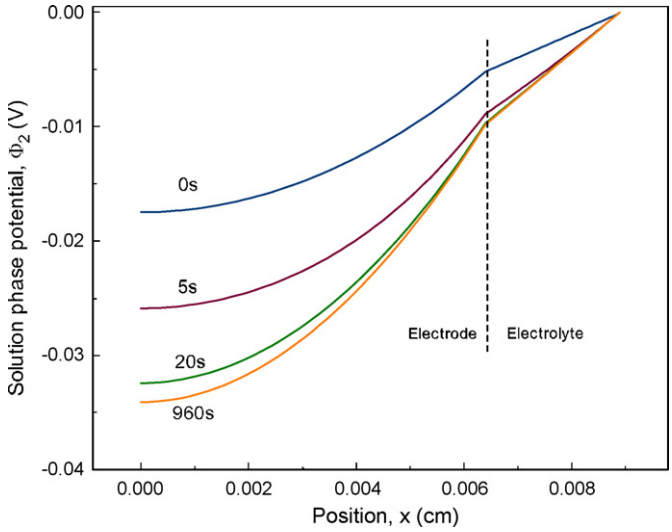

Fig. 17. Calculated solution phase potential distribution at 2 C discharge rate.

trolyte is around 2.5×10^{-6} cm^2 s^{-1} which is several orders of magnitude higher than solid phase diffusion coefficient. The solution phase potential drop across the cell remains near 35 mV throughout the discharge. So neither concentration polarization nor solution phase potential drop substantially limits the cell performance. The solid phase concentration profiles within particles at the electrode–electrolyte interface are shown in Fig. 18 for 2 C discharge process. The large concentration gradient inside the particle at the end of discharge indicates strong solid phase diffusion limitation existing in the electrode.

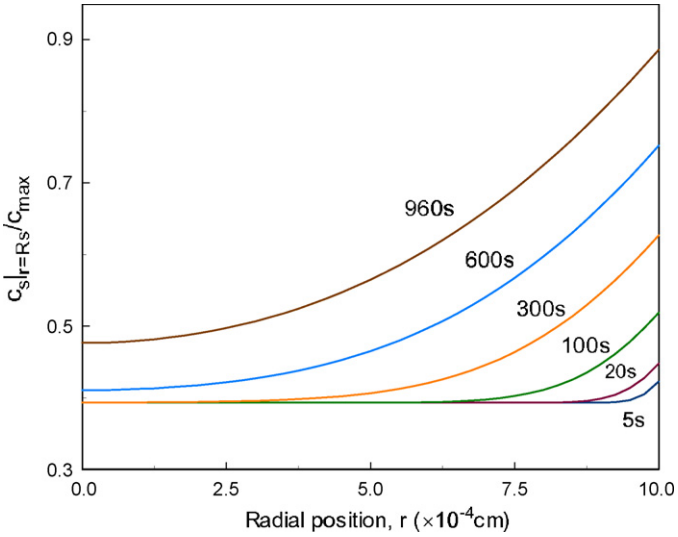

Fig. 18. Calculated solid phase concentration profiles in the half cell at 2 C discharge rate.

5. Conclusion

Rate capability study on a $LiCoO_2$ electrode shows that the discharge behaviors of the $LiCoO_2$ electrode are quite different from its charge behaviors. The overpotential of the electrode in galvanostatic discharge depends strongly on cell SOD, but it does not vary much in galvanostatic charge.

A pseudo-2D porous electrode model is first used to simulate the charge profiles of the $LiCoO_2$ electrode. It is found that the model predicts false potential profiles at the beginning of charge, which is corrected by assuming charge kinetics does not depend on the surface concentration of empty sites in $LiCoO_2$ particle, similar as desorption kinetics. With only constant model parameters, the model predicts potential profiles in good agreement with experimental ones.

Extensive simulations show that the pseudo-2D model has difficulty to predict experimental discharge profiles of the $LiCoO_2$ electrode when model parameters are kept constant. Therefore, symmetry factor in Butler–Volmer equation is empirically assumed to decrease with cell SOD to account for increased potential drop during galvanostatic discharge. It means that the insertion of Li^+ into $LiCoO_2$ electrode becomes kinetically less favorable during discharge, which requires an increased overpotential to maintain the constant discharge current forced by the external circuit. Simulation results from the semi-empirical discharge model are significantly improved and match to experimental discharge profiles well. The model should yield sufficient good results for electrode analysis given that operation conditions of the electrode are not varied to the extent that the empirical representation becomes substantially inaccurate.

Acknowledgement

The authors are grateful for the financial support of the project by the National Reconnaissance Office (NRO) under contract # NRO-000-03-C-0122.

References

[1] M. Doyle, Y. Fuentes, J. Electrochem. Soc. 150 (2003) A706.
[2] P. Ramadass, B. Haran, P.M. Gomadam, R.E. White, B.N. Popov, J. Electrochem. Soc. 151 (2004) A196.
[3] G. Ning, R.E. White, B.N. Popov, Electrochim. Acta 51 (2006) 2012.
[4] J.S. Newman, K.E. Thomas-Alyea, Electrochemical Systems, 3rd ed., Prentice-Hall, Eaglewood Cliffs, NJ, 2004.
[5] M. Doyle, T.F. Fuller, J. Newman, J. Electrochem. Soc. 140 (1993) 1526.
[6] T.F. Fuller, M. Doyle, J. Newman, J. Electrochem. Soc. 141 (1994) 1.
[7] J.N. Reimers, J.R. Dahn, J. Electrochem. Soc. 139 (1992) 2091.
[8] T. Ohzuku, A. Ueda, J. Electrochem. Soc. 141 (1994) 2973.
[9] M. Inaba, Y. Iriyama, Z. Ogumi, Y. Todzuka, A. Tasaka, J. Raman Spectrosc. 28 (1997) 613.
[10] L.O. Valoen, J.N. Reimers, J. Electrochem. Soc. 152 (2005) A882.